Engineering Structures 198 (2019) 109432

Contents lists available at ScienceDirect

Engineering Structures

journal homepage: www.elsevier.com/locate/engstruct

Flexural analysis and design of stainless steel reinforced concrete beams

Musab Rabi[a,b,*], K.A. Cashell[a], R. Shamass[c]

[a] Dept of Civil and Environmental Engineering, Brunel University London, UK
[b] Dept of Civil Engineering, Jerash University, Jordan
[c] Division of Civil and Building Services Engineering, School of Build Environment and Architecture, London South Bank University, UK

ARTICLE INFO

Keywords:
Stainless steel reinforcement
Reinforced concrete
Design methods
Numerical modelling
Continuous strength method
Flexural behaviour

ABSTRACT

The use of stainless steel reinforcement in concrete structures has increased in recent years, particularly in applications where corrosion and chemical resistance is desirable such as bridges, retaining walls and tunnels. Stainless steel has a wide range of attractive properties including excellent mechanical strength, fire resistance, durability and also a long life-cycle compared with carbon steel. However, it is also has a higher initial cost, and therefore needs to be used carefully and efficiently. The existing material models provided for the structural analysis of reinforced concrete members in current design standards, such as Eurocode 2, are not appropriate for stainless steel reinforced concrete and lead to overly conservative (or indeed unconservative in some cases) predictions of the section capacity. Generally, there is a lack of data in the public domain regarding the behaviour of concrete beams reinforced with stainless steel, mainly owing to this being a relatively new and novel topic. In this context, the current paper provides a detailed background of the existing information on stainless steel reinforced concrete, as well a discussion on the potential advantages and challenges. Then, attention is given to analysing the behaviour of stainless steel reinforced concrete beams by developing the Continuous Strength Method to predict the bending moment capacity. A finite element model has been develop in order to further assess the performance, and this is also used to conduct a parametric study of the most influential properties. It is concluded that the proposed analytical models provides a reliable solution for predicting the capacity of concrete beams reinforced with stainless steel.

1. Introduction

Stainless steel is widely used for load-bearing applications in structural engineering, largely owing to its excellent corrosion resistance. In addition to durability, it has a long life-cycle, excellent mechanical characteristics, good formability and recyclability and requires little maintenance. Stainless steel offers excellent ductility and strain hardening capacity compared with traditional carbon steel, which is particularly desirable in design as a ductile section provides warning of imminent collapse. These distinctive properties depend on the constituent elements of the stainless steel alloy, and therefore it is important to select the appropriate grade for each application. One of the most important chemical elements in all stainless steel alloys is chromium which provides the corrosion resistance through the formation of a thin chromium oxide film on the surface of the material in the presence of oxygen, resulting in a passive protective layer [1].

The earliest use of stainless steel in construction was in the 1920s, for roofing and facade applications [2]. In more recent times, stainless steels have become popular in load-bearing applications where the durability, ductility, stiffness and strength are required, as well as excellent fire resistance. Stainless steels are produced in different forms including sheet, plate, bar, tube, hot-rolled and cold-formed structural sections, fasteners and fixings. Cold-formed sections fabricated from steel plates are the most commonly used products for structural members because they are the most readily available and are reasonably straight-forward to manufacture [3].

There are five main categories of stainless steel which are classified according to their metallurgical structure, including the austenitic, ferritic, duplex, martensitic and precipitation hardened grades. The austenitic and duplex grades are most common in structural applications, including for stainless steel reinforcement. Austenitic stainless steels comprise 17–18% chromium and offer very good corrosion resistance, while the duplex grades comprise 22–23% chromium and have even greater strength and corrosion resistance. The characteristic mechanical behaviour of stainless steel is quite different from that of carbon steel in that it does not have the typical yield plateau which is found in carbon steel and also exhibits a predominantly non-linear response with significant strain hardening and high ductility. Extensive

* Corresponding author at: Dept of Civil and Environmental Engineering, Brunel University London, UK.
E-mail address: Mus'ab.Rabi@brunel.ac.uk (M. Rabi).

https://doi.org/10.1016/j.engstruct.2019.109432
Received 12 April 2019; Received in revised form 8 July 2019; Accepted 22 July 2019
Available online 14 August 2019

research into the behaviour of structural stainless steel has been reported in the literature including the flexural behaviour (e.g. [4–6]), compressive behaviour (e.g. [7–9]) and the mechanical characteristics (e.g. [10,11]).

Although there has been extensive research in recent years into the behaviour of structural stainless steel, most of this has been on bare stainless steel sections, rather than reinforced concrete, which is the focus of the current work. Reinforced concrete (RC) structures are widely used for a range of applications such as multi-storey buildings, tunnels and bridges owing to the efficient use and ready availability of the constituent materials. There are increasing demands to improve the life-cycle cost of these types of structure because of the high maintenance costs associated with corrosion of the steel reinforcement and carbonation and deterioration of the concrete. This is particularly true for structures subjected to harsh environments such as in marine, coastal or industrial settings. In this context, the use of stainless steel reinforcement in exposed structures like bridges, retaining walls and tunnels can provide an ideal solution to the deterioration and corrosion problems. This may even result in the structure not requiring expensive inspection and rehabilitation works over its lifetime. Stainless steel reinforcement can also be used for the restoration and rehabilitation of existing concrete structures [12].

It is clear that one of the fundamental advantages of using stainless steel reinforcement in concrete structures is its ability to enhance the durability. For structures reinforced with traditional carbon steel and subjected to aggressive conditions, corrosion is difficult to avoid. The typical approach to improving the durability of RC structures is to change some of the design parameters such as the thickness of the concrete cover or to control the alkalinity of the concrete mix [13]. However, in aggressive conditions, these measures may not be enough to prevent unacceptable levels of corrosion developing. The initial cost of stainless steel reinforcing bars is relatively high, typically between 4 and 8 times than that of traditional carbon steel rebar, depending on the grade. In spite of this, it has been shown that stainless steel reinforcement can reduce the overall maintenance costs during the service life by up to 50%, especially for bridges and marine structures [14,15]. There is a need for a more detailed analysis of the life-cycle costs and savings that using stainless steel reinforced concrete may offer, relative to carbon steel.

Current design codes such as Eurocode 2 do not incorporate an efficient approach for designing structures with stainless steel reinforcement as the given material models for the reinforcement do not fully exploit the significant strain hardening characteristics and high levels of ductility that are present for stainless steel. Given the high initial cost of stainless steel, it is imperative that structurally efficient design solutions are made available which consider and exploit the distinctive and advantageous properties of stainless steel. The Continuous Strength Method (CSM) has been developed in recent years to improve the efficiency and accuracy of design. The CSM was originally developed for stainless steel sections [16] but has been developed in recent years to assess composite beams [17,18]. In the current paper, the main objective is to develop the CSM for stainless steel reinforced concrete sections, exploiting the strain hardening characteristics of the rebars, and to further analyse the behaviour through finite element modelling.

2. Concrete structures with stainless steel reinforcement

It is now recognised that reinforced concrete with carbon steel reinforcement may not be as durable in all conditions as was previously assumed [19]. In harsh environments such as marine or coastal locations, corrosion of carbon steel reinforcement can result in very expensive, challenging and inconvenient rehabilitation works. In this context, stainless steel reinforcement offers a durable and efficient alternative. One of the earliest examples of the use of stainless steel reinforcement is the Progresso Pier in Mexico, as shown in Fig. 1, which was constructed in the early 1940s using grade 1.4301 austenitic

Fig. 1. The Progresso Pier in Mexico [21].

stainless steel. It has been in continuous service for over 70 years without any major repair or significant maintenance activities. The benefits of using stainless steel rebar are quite starkly visible in this image as, in the foreground, the remains of a carbon steel reinforced concrete pier are evident. This was built many years after the stainless steel reinforced concrete pier, but is clearly no longer in service.

Stainless steel reinforcement has also been used in a number of other projects, including Stonecutters Bridge in Hong Kong and Sheik Zayed Bridge in Abu Dhabi, as shown in Figs. 2 and 3, respectively. These two bridges are reinforced with grade 1.4462 duplex stainless steel. Because of the relatively high initial cost, the stainless steel rebars are strategically placed and only used for the outer layer of the reinforcement in both projects, in the so-called splash zone. Grade 1.4436 stainless steel was used in the Highnam bridge widening project in the UK as well as the Broadmeadow Bridge in Ireland. One of the most high profile and recent applications of stainless steel rebar is in the Queensferry Crossing in Scotland which opened in 2017. As well as new construction, stainless steel reinforcement has also been used for renovation and restoration purposes. For example, austenitic grade 1.4301 stainless steel rebar was used to rehabilitate the pillars and stone arches of the Knucklas Rail Bridge [20].

In the design of reinforced concrete beams, Eurocode 2 assumes that the compression forces are resisted entirely by the concrete whereas the steel reinforcement carries the tension. The tensile strength of concrete is difficult to measure accurately and represents only about 10% of the compressive strength, so its contribution is usually ignored. Fig. 4 shows (a) a typical simple RC cross-section together with the corresponding (b) strain and (c and d) stress distributions, as assumed in Eurocode 2. In these figures, b and h are the width and depth of the beam, respectively, and y and d are the locations of the neutral axis and steel reinforcement from the top fibre of the beam, respectively. The strain in the concrete at the outer fibre is ε_c whereas ε_s is the reinforcement strain, and f_c and σ_s are the compressive stress of the concrete and tensile stress in the reinforcement, respectively. The failure mechanisms considered are either crushing of the concrete (i.e.

Fig. 2. Stonecutters bridge in Hong Kong [22].

Fig. 3. Sheik Zayed bridge in Abu Dhabi [23].

when the strain at the outer fibre of the concrete reaches the ultimate crushing strain) or yielding of the reinforcement (i.e. when the strain in the steel reinforcement reaches its yield value). In accordance with the stress blocks presented in Fig. 4(d), any contribution to the load capacity after the steel yield strength has been reached, is not considered in design. Currently, the majority of global design standards including Eurocode 2 do not fully exploit strain hardening of the reinforcement in the plastic design of RC structures. Although this assumption is acceptable for carbon steel reinforced concrete, it can give inaccurate predictions when stainless steel reinforcement is used since it exhibits very different stress-strain behaviour in that it is nonlinear from an early stage and develops significant levels of strain hardening. For this reason, designing stainless steel RC structures using the existing design rules is neither efficient nor reflective of the real behaviour. It is in this context that the current work is undertaken and a new approach for the design of reinforced concrete structures with stainless steel rebar is developed.

3. Design of stainless steel reinforced concrete beams

3.1. Background to the Continuous Strength Method

The Continuous Strength Method (CSM) is a deformation-based design method which has been developed in recent years to enable material strain hardening properties to be exploited, thus resulting in more accurate capacity predictions and more efficient design. The CSM was originally developed for the design of stainless steel members with non-slender cross-sections [16]. Since then, it has been extended many times to cover the design of structural members made from stainless steel (e.g. [9,24]), carbon steel (e.g. [17,25–27]), aluminium [28] and high strength steel [29]. In recent years, the method has been adapted for composite construction including carbon steel-concrete composite beams [17] and stainless steel-concrete composite members with either a full and partial shear connection [18]. The CSM is based on replacing traditional cross-section classification with an assessment of the deformation capacity of the section, using a realistic material model. As such, the method predicts the cross-sectional resistance of the member depending on two main components: (1) a base curve that defines the relationship between the limiting strain at the ultimate load and the cross-section slenderness, and (2) a material model that allows for strain hardening [30].

In the current paper, a similar approach is adopted to develop a deformation-based design method for reinforced concrete beams with stainless steel rebar, allowing for the true stainless steel constitutive relationship. This is developed in two forms, first as a full model in which the whole material response is captured and then as a simplified model incorporating a more simplistic elastic-linear hardening stainless steel constitutive response.

3.2. Material model

The full and simplified version of the proposed CSM design model use two different material models for representing the stainless steel reinforcement. As stated previously, the stress-strain behaviour of stainless steel is quite different from that of carbon steel. Carbon steel has a linear elastic response with a well-defined yield point and yield plateau, followed by a moderate degree of strain hardening. On the other hand, stainless steel exhibits a predominantly non-linear and continuous stress-strain response without a clearly-defined yield point as well as significant levels of strain hardening. In the absence of a visible yield point, the typical value adopted is the 0.2% proof stress ($\sigma_{0.2}$) which is determined by drawing a line with a slope equal to the elastic modulus (E) between 0.2% strain on the x-axis and the stress-strain curve.

The full CSM analysis employs the modified Ramberg-Osgood stainless steel material model [10,11,31], as depicted in Fig. 5. This uses the original expression proposed by Ramberg–Osgood [10], as presented in Eq. (1), to define the stress-strain relationship of stainless steel up to the proof stress followed by Eq. (2) [11,31] for greater levels of stress.

$$\varepsilon = \frac{\sigma}{E} + 0.002\left(\frac{\sigma}{\sigma_{0.2}}\right)^{n} \tag{1}$$

$$\varepsilon = \varepsilon_{0.2} + \frac{\sigma - \sigma_{0.2}}{E_2} + \left(\varepsilon_u - \varepsilon_{0.2} - \frac{\sigma_u - \sigma_{0.2}}{E_2}\right)\left(\frac{\sigma - \sigma_{0.2}}{\sigma_u - \sigma_{0.2}}\right)^{m} \quad \text{for } \sigma_{0.2} < \sigma \leq \sigma_u \tag{2}$$

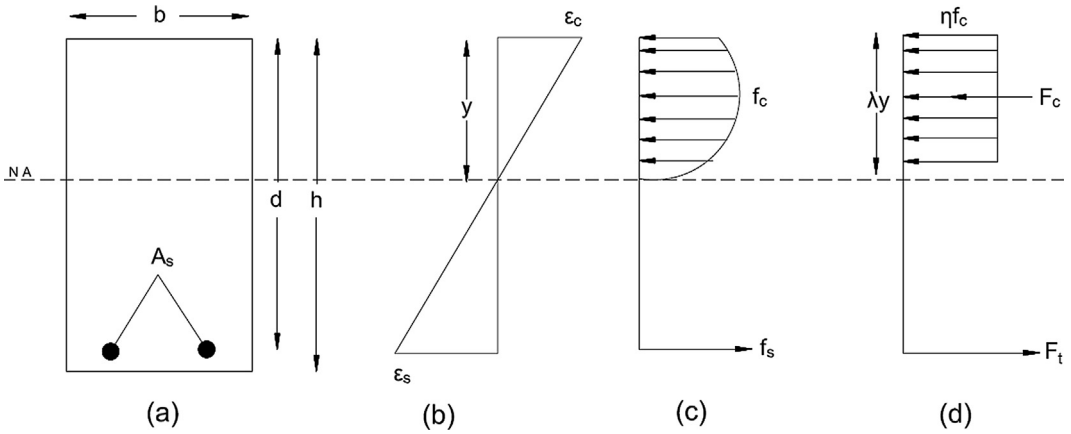

Fig. 4. Strain and stress distribution diagrams for a singly reinforced concrete beam including (a) the cross-section (b) the strain distribution through the section, (c) the stress distribution and (d) an equivalent stress distribution in the section, simplifying the concrete stress block.

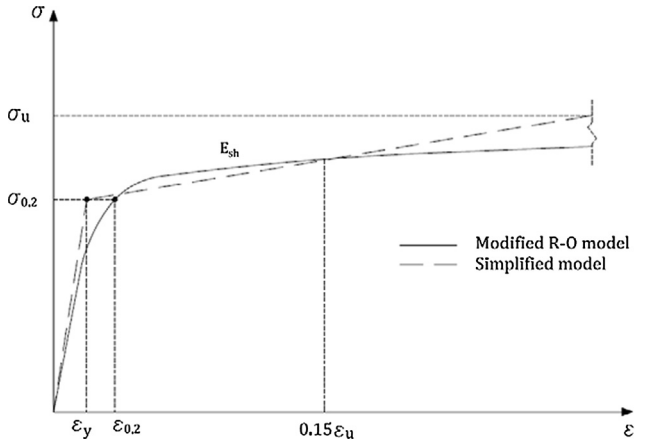

Fig. 5. The simplified material model for stainless steel with reference to the modified R-O model.

In these expressions, ε and σ are the engineering strain and stress, respectively, E_2 is the tangent modulus at the 0.2% proof stress point, σ_u and ε_u are the ultimate stress and corresponding strain, respectively, $\varepsilon_{0.2}$ is the strain corresponding to $\sigma_{0.2}$ and n and m are model constants related to the strain hardening behaviour.

The simplified CSM employs a bilinear, elastic-linear hardening stress-strain relationship for the stainless steel rebar, as shown in Fig. 5, in order to avoid the need to solve complex nonlinear equations. In this approach, the yield point is identified as the 0.2% proof stress and the corresponding yield strain (i.e. $\sigma_{0.2}$ and $\varepsilon_y = \frac{\sigma_{0.2}}{E}$, respectively). The slope of the strain hardening region (E_{sh}) is obtained from the line passing through the yield point (ε_y, $\sigma_{0.2}$) and the defined ultimate point ($C_2\varepsilon_u$, σ_u), as defined in Eq. (3). It has been found that a value of 0.15 is an appropriate value for the constant C_2 in the current work, in agreement with previous CSM developments [9].

$$E_{sh} = \frac{\sigma_u - \sigma_{0.2}}{C_2\varepsilon_u - \varepsilon_y} \tag{3}$$

3.3. Flexural capacity of stainless steel reinforced concrete beams

3.3.1. Full analytical model

In this section, the Continuous Strength Method (CSM) is developed to analyse the behaviour of stainless steel reinforced concrete beams, using the modified Ramberg-Osgood relationship described in Eqs. (1) and (2) to model the rebars. The plastic bending moment capacity is obtained by locating the neutral axis (NA) and then applying the equilibrium of internal force equations to the cross-section of the beam. In order to idealise the behaviour, the following assumptions are made in the analytical model, in accordance with Eurocode 2:

(1) The nominal ultimate strain of the concrete (ε_{cu}) is assumed to be 0.0035 for material with a compressive strength less than 50 N/mm^2, otherwise it is determined using Eq. (4):

$$\varepsilon_{cu} = 2.6 + 35[(98 - f_c)/100]^4 \tag{4}$$

(2) As presented in Fig. 4 (d), an equivalent rectangular stress distribution is assumed for the concrete in compression. The effective strength of the concrete is $0.85f_c$, where f_c is the compressive strength of the concrete, and the effective height of the compression zone is 0.8y, where y is the distance from the NA to the top fibre of the cross-section.

The material model for stainless steel given in Eqs. (1) and (2) provides strain as a function of stress. However, in order to implement the material model in conjunction with the design method, it is necessary to identify the stress as a function of strain, which requires a numerical procedure. In the current work, the approximate inversion relationship proposed by Abdella [32] for the full stress-strain relationship of stainless steel is employed to describe the stress (σ) as an explicit function of strain (ε), as presented in the Eqs. (5) and (6):

$$\sigma_1(\varepsilon) = \sigma_{0.2}\frac{r\left(\frac{\varepsilon}{\varepsilon_{0.2}}\right)}{1 + (r-1)\left(\frac{\varepsilon}{\varepsilon_{0.2}}\right)^p} \quad \text{for} \quad \varepsilon \le \varepsilon_{0.2} \tag{5}$$

$$\sigma_2(\varepsilon) = \sigma_{0.2}\left[1 + \frac{r_2\left[\frac{\varepsilon}{\varepsilon_{0.2}} - 1\right]}{1 + (r^* - 1)\left(\frac{\frac{\varepsilon}{\varepsilon_{0.2}} - 1}{\frac{\varepsilon_u}{\varepsilon_{0.2}} - 1}\right)^{p^*}}\right] \quad \text{for} \quad \varepsilon > \varepsilon_{0.2} \tag{6}$$

where the material parameters are:

$$\varepsilon_{0.2} = \frac{\sigma_{0.2}}{E} + 0.002 \qquad r = \frac{E\varepsilon_{0.2}}{\sigma_{0.2}}$$

$$E_2 = \frac{E}{1 + 0.002n/e} \qquad p = r\frac{1 - r_2}{r - 1}$$

$$e = \frac{\sigma_{0.2}}{E} \qquad m = 1 + 3.5\frac{\sigma_{0.2}}{\sigma_u}$$

$$\sigma_u = \sigma_{0.2}\frac{1 - 0.0375(n - 5)}{0.2 + 185e} \qquad E_u = \frac{E_2}{1 + (r^* - 1)m}$$

$$r_2 = \frac{E_2\varepsilon_{0.2}}{\sigma_{0.2}} \qquad r_u = \frac{E_u(\varepsilon_u - \varepsilon_{0.2})}{\sigma_u - \sigma_{0.2}}$$

$$\varepsilon_u = \min(1 - \frac{\sigma_{0.2}}{\sigma_u}, A) \qquad p^* = r^*\frac{1 - r_u}{r^* - 1}$$

$$r^* = \frac{E_2(\varepsilon_u - \varepsilon_{0.2})}{\sigma_u - \sigma_{0.2}}$$

In these expressions, A is the stainless steel elongation, E_2 and E_u are the slope of the stress-strain curve at $\varepsilon_{0.2}$ and ε_u, respectively, and r, r_2, r*, r_u, p, p* and m are parameters that need to be determined.

For calculating the bending moment capacity of a singly reinforced beam, there are two possible cases. Case 1 is when the tensile strain of the reinforcement is less than the total strain corresponding to $\sigma_{0.2}$ (i.e. $\varepsilon_s \le \varepsilon_{0.2}$) and Case 2 is when the tensile strain of the reinforcement is greater than the total strain corresponding to $\sigma_{0.2}$ (i.e. $\varepsilon_s > \varepsilon_{0.2}$). The internal tensile and compressive forces in the cross-section are calculated based on the full stainless steel stress-strain material model and the equivalent rectangular compressive stress distribution in the concrete, together with the strain distribution in the section. In order to determine the tensile stress in the reinforcement at failure of the beam, the strain can be calculated from the strain distribution in Fig. 4(b), as follows:

$$\varepsilon_s = \kappa(d - y) \tag{7}$$

$$\kappa = min(\kappa_{su}, \kappa_{cu}) \tag{8}$$

where κ_{su} is the limiting curvature for stainless steel failure and κ_{cu} is the limiting curvature for concrete failure (i.e. when the strain at the top fibre of the beam reaches the ultimate strain of concrete). There are two possible failure models, defined by κ_{su} and κ_{cu}. If $\kappa_{su} < \kappa_{cu}$, the beam fails due to rupture of the stainless steel reinforcement whereas if $\kappa_{su} > \kappa_{cu}$, the reinforced beam fails due to concrete crushing. The values of κ_{su} and κ_{cu} are determined as:

$$\kappa_{su} = \frac{\varepsilon_u}{d - y}$$

$$\kappa_{cu} = \frac{\varepsilon_{cu}}{y} \tag{9}$$

From equilibrium of the internal forces in the beam, the sum of the tensile forces (F_t) and the compression forces (F_c) must equal zero:

$$F_c - F_t = 0 \tag{10}$$

The tension force is determined as the product of the steel area (A_s) and the stress in the stainless steel (σ_s):

$$F_t = A_s\sigma_s \tag{11}$$

and the compression force is found using the equivalent rectangular stress block presented in Fig. 4(d), to give:

$$F_c = 0.85f_c(0.8y)b \tag{12}$$

Substituting Eq. (12) and Eq. (11) into Eq. (10) gives:

$0.68f_cyb - A_s\sigma_s = 0$ or

$$y = \frac{A_s\sigma_s}{0.68f_cb} \tag{13}$$

When the stainless steel strain is less than $\varepsilon_{0.2}$ (i.e. $\varepsilon_s \le \varepsilon_{0.2}$), the tensile stress in the reinforcement at d is determined by substituting Eq. (7) into Eq. (5) to give:

$$\sigma_s = \sigma_1(y) = \sigma_{0.2}\frac{r\left(\frac{\kappa(d-y)}{\varepsilon_{0.2}}\right)}{1 + (r-1)\left(\frac{\kappa(d-y)}{\varepsilon_{0.2}}\right)^p} \tag{14}$$

which can be used together with Eq. (13) to obtain y, the depth of the neutral axis measured from the top fibre of the beam. Since the stress $\sigma_1(y)$ is a nonlinear function of the variable y, Eqs. (13) and (14) create a nonlinear problem which must be solved using an iterative method. Once the position of the neutral axis, y, is located, the assumption of $\varepsilon_s \le \varepsilon_{0.2}$ must be checked by calculating the strain in the stainless steel using Eq. (7). If the assumption is correct, the plastic bending moment capacity of the beam is calculated by taking moments about the position that the compressive internal force in the concrete acts, as follows:

$$M_{pl} = A_s\sigma_s(d - 0.4y) \tag{15}$$

where σ_s is the tensile stress in the stainless steel calculated from Eq. (14) and corresponding to the obtained neutral axis depth, y.

If the stainless steel strain is higher than the strain corresponding to $\sigma_{0.2}$ (i.e. $\varepsilon_s > \varepsilon_{0.2}$), the tensile stress of the reinforcement can be obtained by substituting Eq. (7) into Eq. (6) to give:

$$\sigma_s = \sigma_2(y) = \sigma_{0.2}\left[1 + \frac{r_2\left(\frac{\kappa(d-y)}{\varepsilon_{0.2}} - 1\right)}{1 + (r^* - 1)\left(\frac{\frac{\kappa(d-y)}{\varepsilon_{0.2}} - 1}{\frac{\varepsilon_u}{\varepsilon_{0.2}} - 1}\right)^{p^*}}\right] \tag{16}$$

The position of the neutral axis (y) can then be obtained, as before, using the equilibrium of internal forces (i.e. Eq. (13)) and substituting the tensile stress obtained from Eq. (16) into Eq. (13). Once the position of neutral axis is known, the plastic bending capacity is calculated by taking moments about the position of the compression force, and is given in the Eq. (15). As before, σ_s is the tensile stress in the stainless steel calculated from Eq. (16) and corresponding to the calculated value of y. A flow chart presenting the full procedure for determining the neutral axis and the plastic bending moment capacity is given in Fig. 6.

3.3.2. Simplified analytical model

In the previous section, a detailed analytical solution was presented to predict the plastic bending moment capacity of stainless steel reinforced concrete beams, incorporating the full stress-strain behaviour of the stainless steel material. This method involves a solution of complex nonlinear equations requiring iterative methods to obtain the position of the neutral axis, which may not be a straightforward procedure for designers. Therefore, in this current section, a simplified analytical solution is developed based on a simpler material model for the stainless steel, as described in Section 3.2 and Fig. 5. The other initial assumption in the simplified model is that the section always fails due to concrete crushing (i.e. $\kappa_{su} > \kappa_{cu}$), which is a legitimate assumption generally for reinforced concrete beams, and even more so for those reinforced with stainless steel rebar owing to its ductility. Hence, the tensile strain of the reinforcement at the failure of the section is determined from the strain distribution in Fig. 4(b) as follows:

$$\varepsilon_s = \frac{\varepsilon_{cu}}{y}(d - y) \tag{17}$$

The tensile stress of the stainless steel can be calculated from the simplified material model presented in Fig. 5, in accordance with Eqs (18) and (19) hereafter:

$$\sigma_s = E\varepsilon_s \quad \varepsilon_s \le \varepsilon_y \tag{18}$$

$$\sigma_s = \sigma_{0.2} + E_{sh}(\varepsilon_s - \varepsilon_y) \quad \varepsilon_s > \varepsilon_y \tag{19}$$

There are two possible cases for prediction of the bending moment capacity of reinforced beam. Case 1 is when the tensile strain of the reinforcement is less than the yield strain (i.e. $\varepsilon_s \le \varepsilon_y$) and Case 2 is when the tensile strain of the reinforcement is higher than the yield strain (i.e. $\varepsilon_s > \varepsilon_y$). For Case 1, when the strain in the stainless steel is less than ε_y (i.e. $\varepsilon_s \le \varepsilon_y$), the tensile stress in the reinforcement at d is determined by substituting Eq. (17) into Eq. (18) to give:

$$\sigma_s = E\frac{\varepsilon_{cu}}{y}(d - y) \tag{20}$$

which can be used together with Eq. (13) to give:

$$0.68f_cyb - A_sE\frac{\varepsilon_{cu}}{y}(d - y) = 0 \tag{21}$$

This can be simplified to Eq. (22):

$$0.68f_cby^2 + A_s\varepsilon_{cu}Ey - A_s\varepsilon_{cu}dE = 0 \tag{22}$$

Once the position of the neutral axis (y) is located by solving this quadratic equation, the assumption of $\varepsilon_s \le \varepsilon_y$ must be checked by calculating the strain in the stainless steel using Eq. (17). If the assumption is correct, the plastic bending moment capacity of the beam is calculated by taking moments about the position of the compressive internal force in the concrete using Eq. (15) where σ_s is the tensile stress in the stainless steel calculated from Eq. (20).

If the stainless steel strain is higher than the yield strain (i.e. $\varepsilon_s > \varepsilon_y$), the tensile stress of the reinforcement can be obtained by substituting Eq. (17) into Eq. (19) to give:

$$\sigma_s = \sigma_{0.2} + E_{sh}\left(\frac{\varepsilon_{cu}}{y}(d - y) - \varepsilon_y\right) \tag{23}$$

As before, the position of the neutral axis is located using the equilibrium of the internal forces by substituting the tensile stress obtained from Eq. (23) into Eq. (13) to give:

$$0.68f_cyb - A_s\left(\sigma_{0.2} + E_{sh}\left(\frac{\varepsilon_{cu}}{y}(d - y) - \varepsilon_y\right)\right) = 0 \tag{24}$$

This can simplified, as follows:

$$0.68f_cby^2 + (E_{sh}\varepsilon_{cu} + E_{sh}\varepsilon_y - \sigma_{0.2})A_sy - A_sE_{sh}\varepsilon_{cu}d = 0 \tag{25}$$

Once the position of the neutral axis is located using Eq. (25), the plastic bending moment capacity is calculated as given in Eq. (15) where σ_s is the tensile stress in the stainless steel calculated from Eq. (23). In both cases, the assumption of $\kappa_{su} > \kappa_{cu}$ must be checked to ensure that the beam section fails due to concrete crushing.

In the case that the limiting curvature for stainless steel is less than that of the concrete (i.e. $\kappa_{su} > \kappa_{cu}$), the beam fails due to the rupture of stainless steel reinforcement, which should be very rare in reality. In this scenario, the tensile strain of the reinforcement at failure of the section is its ultimate tensile strain, as given in Eq. (26):

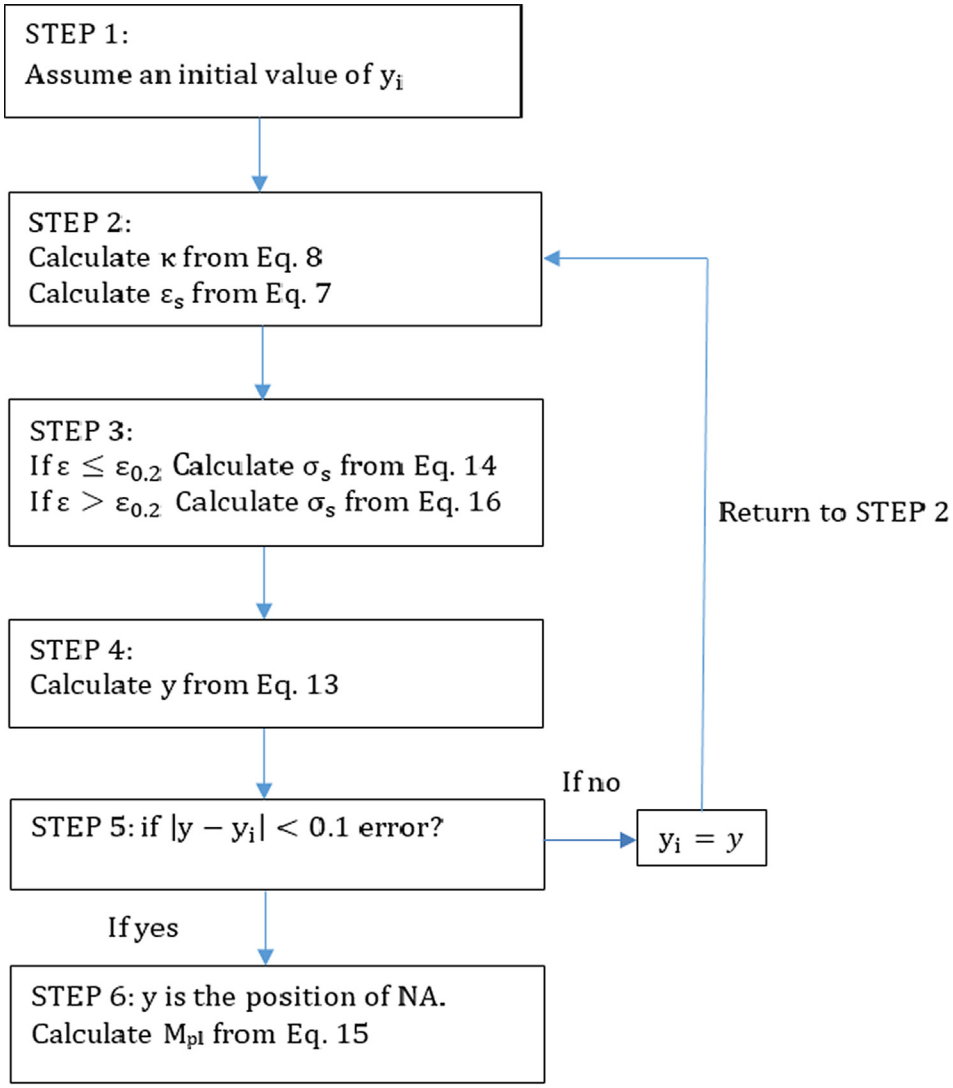

Fig. 6. Flow chart of the solution procedure for a singly reinforced concrete beam.

$$\varepsilon_s = \varepsilon_u \tag{26}$$

The tensile stress of the stainless steel is determined by substituting Eq. (26) in to Eq. (19) to give:

$$\sigma_s = \sigma_{0.2} + E_{sh}(\varepsilon_u - \varepsilon_y) \tag{27}$$

As before, the position of the neutral axis is located by applying the equilibrium of internal forces criteria, and substituting the tensile stress obtained from Eq. (27) into Eq. (13) to give:

$$0.68 f_c y b - A_s(\sigma_{0.2} + E_{sh}(\varepsilon_u - \varepsilon_y)) = 0 \tag{28}$$

Again, once the position of the neutral axis is located using Eq. (28), the plastic bending moment capacity is calculated as given in Eq. (15) where σ_s is the tensile stress in the stainless steel calculated from Eq. (27).

4. Development of the finite element model

A finite element model has been developed using the general purpose finite-element analysis software Abaqus [33] in order to examine the analytical design model described in the previous section, and to conduct further parametric studies. Abaqus offers a number of different solution strategies for complex nonlinear problems and in the current work, an implicit dynamic solution procedure is selected. This can be used efficiently for quasi-static applications and has been shown to provide better convergence behaviour than the modified Riks method for arrangements like those considered herein [34]. In the model, the concrete elements are represented using 3D eight-node hexahedral elements which are known as C3D8 in the Abaqus library whereas the reinforcement is simulated using 2-node beam elements (B3). The reinforcement is embedded in the concrete and the translational degrees of freedom at each node of the reinforcement are constrained to the interpolated values of the corresponding degrees of freedom of the concrete element [33]. A mesh sensitivity study has been conducted to select the most appropriate mesh size and it was found that elements which are 15 mm^3 in size are the most appropriate in terms of achieving both computational accuracy and efficiency. For relatively small beams, a smaller element size of 10 mm^3 is used.

4.1. Material behaviour

4.1.1. Concrete

A number of concrete material models are available in Abaqus including the smeared crack concrete model and the concrete damage plasticity (CDP) model. The former is based on reducing the stiffness of concrete elements when the stresses exceed the maximum tensile stress, while the latter considers the inelastic behaviour of concrete by defining damage factors in both compression and tension. The CDP model is selected in this study for simulating the concrete behaviour as it is

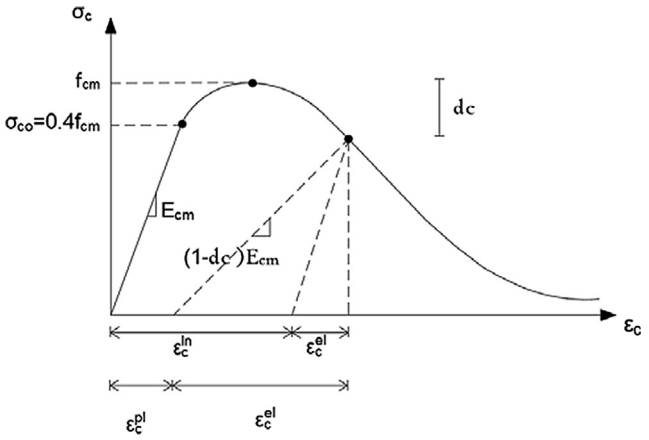

Fig. 7. CDP model for concrete in compression [33].

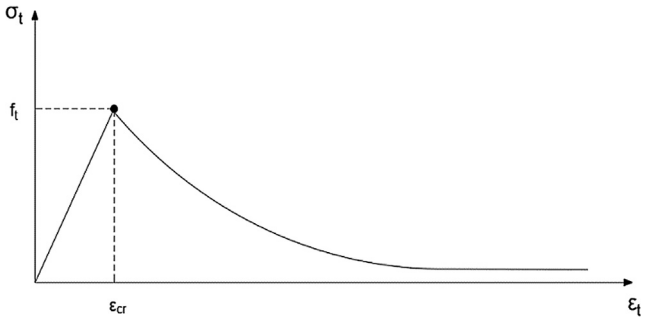

Fig. 8. Post-failure stress-strain relationship proposed by [40].

more desirable in applications where the concrete is subject to static loads and has been used widely for similar applications in the literature [e.g. 35–38].

The CDP model as shown in Fig. 7 is based on continuum damage mechanics and considers two failure modes, namely cracking of the concrete in tension and crushing in compression. The material behaviour is defined in terms of the elastic, plastic, compressive and tensile properties. In the current work, Poisson's ratio and density of concrete are taken as 0.15 and 2400 kg/m^3, respectively. For the compression behaviour, the model given in Eurocode 2 [39] is adopted, given as:

$$\sigma_c = \left(\frac{k\eta - \eta^2}{1 + (k-2)\eta}\right) f_{cm} \quad \text{for} \quad 0 \le \varepsilon_c \le \varepsilon_{cu1} \tag{29}$$

In this expression, ε_{cu1} is the nominal ultimate strain and f_{cm} is the ultimate compressive strength of concrete (in MPa), given by:

$$f_{cm} = f_{ck} + 8 \tag{30}$$

where f_{ck} is the characteristic cylinder strength. The parameters k and η are determined from Eqs. (31) and (32), respectively:

$$k = 1.05 E_{cm} \frac{\varepsilon_{c1}}{f_{cm}} \tag{31}$$

$$\eta = \frac{\varepsilon_c}{\varepsilon_{c1}} \tag{32}$$

in which E_{cm} is the elastic modulus of concrete (in MPa) and ε_{c1} is the strain at the peak stress, determined from Eqs. (33) and (34):

$$E_{cm} = 22(0.1 f_{cm})^{0.3} \tag{33}$$

$$\varepsilon_{c1} = 0.7(f_{cm})^{0.31} \le 2.8 \tag{34}$$

The nominal ultimate strain (ε_{cu1}), as a percentage, is given by:

$$\varepsilon_{cu1} = 2.8 + 27[(98 - f_{cm})/100]^4 \quad \text{for} \quad f_{ck} \ge 50 \ \text{N/mm}^2, \text{otherwise} 3.5 \tag{35}$$

The CDP model requires the compressive damage parameter (d_c) to be defined at each inelastic strain increment, ranging from 0, for un-damaged material, to 1, when the concrete completely loses its load-bearing capacity. As shown in Fig. 7, this parameter is calculated for the descending branch of the stress-strain curve of concrete in compression as follows:

$$d_c = 0 \quad \text{for} \quad \varepsilon_c < \varepsilon_{c1} \tag{36}$$

$$d_c = \frac{f_{cm} - \sigma_c}{f_{cm}} \quad \text{for} \quad \varepsilon_c \ge \varepsilon_{c1}$$

In tension, the concrete stress-strain behaviour is modelled as a linear relationship up to the ultimate tensile strength (ε_{cr}) followed by a gradually descending branch, which inherently incorporates the effects of tension stiffening (Fig. 8). The effect of the bond between the rebar and the concrete is approximated within this tension stiffening branch. Tension stiffening refers to the phenomenon whereby concrete continues to carry some tensile load even after cracking has taken place, though the tensile strength gradually decreases with increasing tensile strain. This is captured within the descending branch of the concrete stress-strain model which, in Abaqus, can be described using a linear, bilinear or nonlinear relationship. In this study, the power stress-strain relationship proposed by Wang and Hsu [40] is employed for the descending branch, as described in Fig. 8 and presented in Eq. (37). This nonlinear formula has also been used by other researchers in the literature [e.q. 41,42]:

$$\sigma_t = E_{cm}\varepsilon_t \quad \text{if} \quad \varepsilon_t \le \varepsilon_{cr} \tag{37}$$

$$\sigma_t = f_t\left(\frac{\varepsilon_{cr}}{\varepsilon_t}\right)^{0.4} \quad \text{if} \quad \varepsilon_t > \varepsilon_{cr}$$

The tensile strength (f_t) can be obtained as follows [39]:

$$f_t = 0.3(f_{ck})^{2/3} \tag{38}$$

In addition to the compressive and tensile constitutive relationships, a number of other parameters are required in the CDP model. The eccentricity, ratio of the strength in the biaxial state to the strength in the uniaxial state (f_{b0}/f_{c0}), parameter K, and viscosity parameter are obtained from Abaqus manual [33] and set as 0.1, 1.16, 0.667, and 0, respectively, whereas the dilation angle is selected based on a

Table 1
Material properties of the RC beams reported by [43–47].

Beam	Reinforcement					Concrete	
	Material	Diameter (mm)	Young's modulus E (kN/mm^2)	Yield strength $\sigma_{0.2}$ (N/mm^2)	Ultimate strength σ_u (N/mm^2)	Young's modulus E_{cm} (N/mm^2)	Compressive strength f_{ck} (N/mm^2)
B3	Duplex stainless Steel 1.4362	8	189	1003	1066	Not provided	26.6 (cylinder)
SS	Austenitic stainless steel 1.4311	20	177	480	773	37.6	50.0 (cylinder)
SR6	Carbon steel	14	200	410	Not provided	Not provided	31.3 (cube)
U2	Carbon steel	12	205	380	Not provided	26.0	19.4 (cube)
O	Carbon steel	12	209	507	Not provided	Not provided	30.0 (cylinder)

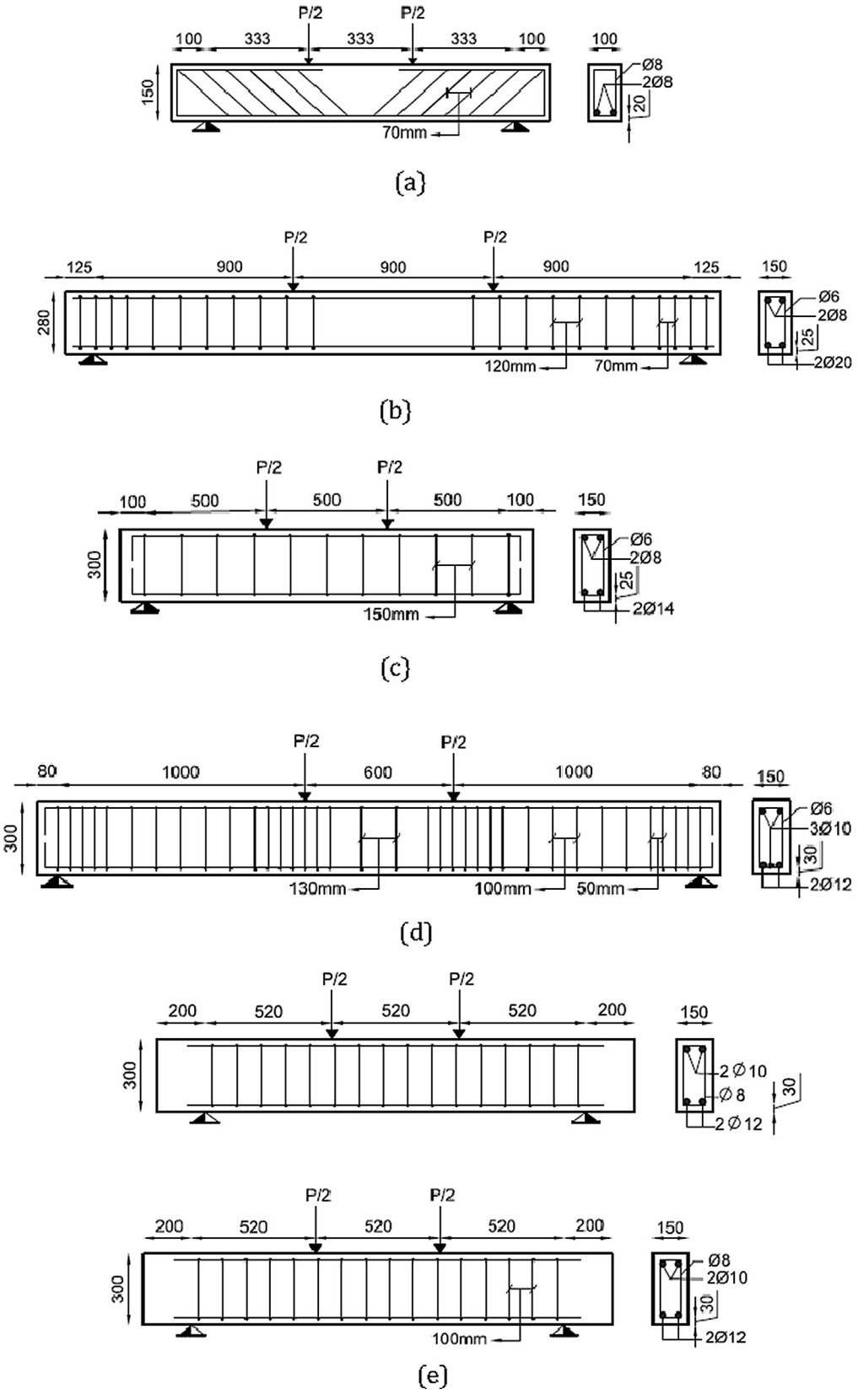

Fig. 9. Geometrical and reinforcement details of the beams used in the validation study, including (a) B3 [43] (b) SS [44], (c) SR6 [45], (d) U2 [46] and (e) O [47].

sensitivity study and set as 36°.

4.1.2. Stainless steel reinforcement

The stainless steel material is represented in the model using the modified Ramberg-Osgood model described earlier and presented in Fig. 5. As stainless steel does not exhibit a clearly defined yield point, the 0.2% proof stress is used to define the yield stress. The stress-strain relationships described in Eqs. (1) and (2) are employed to model the

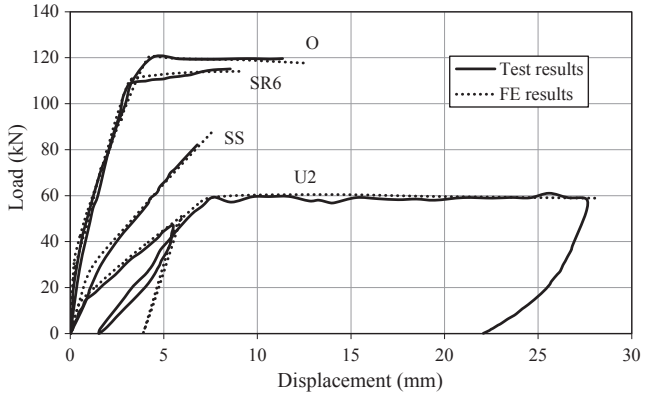

Fig. 10. Comparison between experimental and numerical load-displacement curves for beams SS [44], SR6 [45], U2 [46] and O [47].

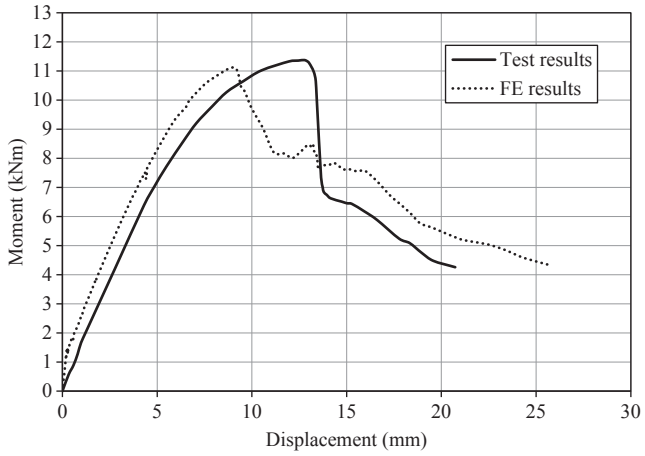

Fig. 11. Comparison between experimental and numerical moment-displacement curves for beam B3 [43].

stainless steel constitutive relationship in Abaqus.

Abaqus requires that the material properties are specified in terms of true stress (σ_{true}) and strain (ε_{true}) which can be derived from the engineering stress-strain curves as follows:

$$\sigma_{true} = \sigma(1 + \varepsilon)$$

$$\varepsilon_{true} = \ln(1 + \varepsilon) \quad (39)$$

4.2. Boundary and loading conditions

The beam model is designed to simulate a four-point bending test arrangement where the loads are applied through a 3 cm wide surface in displacement control. There are pinned boundary conditions and therefore the beam ends are restrained against vertical displacement but allow movement at the other degrees of freedom. As the beam is symmetrical about both its longitudinal axis and along the length, it is only necessary to model a quarter of the beam, and use symmetrical boundary conditions along the length and also around the x- and z-axis at the mid-span to reduce the computational time and cost.

5. Validation of the finite model

5.1. Experimental results for validation

The FE model is validated using five reinforced concrete beams from different experimental programmes, as presented in Table 1. Beams SS and B3 were reinforced with austenitic and duplex stainless steel rebars in grade 1.4311 and 1.4362, respectively. As these are the only two stainless steel reinforced concrete beam tests which have been found in the literature, three other beams containing carbon steel reinforcement are also included in the validation exercise for additional robustness. The details of geometry and reinforcement of these beams are shown in Fig. 9.

All of the beams were tested under monotonic loading, in displacement control. Beams B3, SR6 and O were loaded continuously until failure. On the other hand, beam U2 was loaded until cracking occurred and then unloaded to zero before being reloaded up to failure. Beam SS was subjected to loading up to 80 kN before the test was stopped (the reason for stopping the test at this point is not known but it was possibly owing to the test machine capacity being reached).

Table 1 presents the material properties of the concrete and the reinforcement for each of these beams, as provided in the literature. The elastic modulus and tensile strength of the concrete can be calculated using Eq. (33) and Eq. (38), respectively, for beams where this data was not provided. For beam SS, the exponent of 0.4 in Eq. (37) is changed to 0.3 in order to obtain better depiction of the experimental response. This is most likely because this grade of stainless steel reinforcement has a different bond relationship with the surrounding concrete compared with carbon steel rebar.

5.2. Load-displacement response

Fig. 10 presents the load-displacement curves obtained for beams SS, SR6, U2 and O from the FE model, together with the corresponding experimental data. Fig. 11 presents the moment-displacement curve for beam B3, as this is the manner in which the experimental data is published [43]. With reference to Fig. 10, it is observed that the model presents an excellent depiction of the overall behaviour in all cases. The key features such as initial stiffness, cracking point, and ultimate strength are in very good agreement. For all of the beams, the initial stiffness of the beams is slightly greater in the FE model data compared with the experimental response, most likely due to some localised cracking in the experiment which is not captured in the numerical simulations. For beam U2, the loading-unloading-reloading path is reasonably well simulated by the model although there is some disparity between the residual displacements (i.e. the displacements when the applied load returns to zero following the unloading phase) predicted (around 3.9 mm) and those that occurred in the test (1.53 mm). This is possibly due to differences in the way that the tensile behaviour of concrete is represented in the model, compared with the experimental performance.

The results for Beam B3 presented in Fig. 11 demonstrate that the FE model captures the ultimate moment quite well, with the disparity between the model predictions and the experimental data being around 2%. However, the stiffness response obtained numerically is greater than occurred during the experiment, which is most likely due to localised cracking again that is not captured exactly by the model. Nevertheless, in conclusion, a good agreement has been shown between the numerical load-displacement response and the experimental data.

5.3. Crack pattern

Fig. 12(a) and (b) show the crack patterns obtained numerically and experimentally, respectively, for beam SR6 at the ultimate load, which occurred at a displacement of 3.7 mm (it is noteworthy that the FE model captures the opposite side of the beam than that is represented in Fig. 12(b)). This beam is selected for demonstration purposes and similar comparisons have been found for all of the other beams in this validation study, where the data is available in the literature. In the legend for Fig. 12(a), the term “PE Max Principle” as outputted by Abaqus refer to the tensile plastic strain values in the concrete which represent tensile cracks in the beam. In the FE analysis, two cracks develop in the constant-moment region (i.e. the region between the

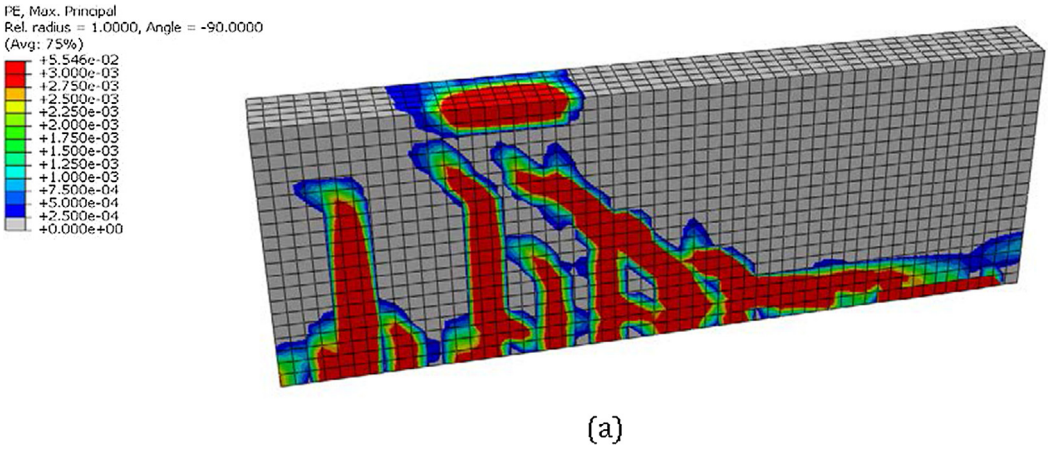

(a)

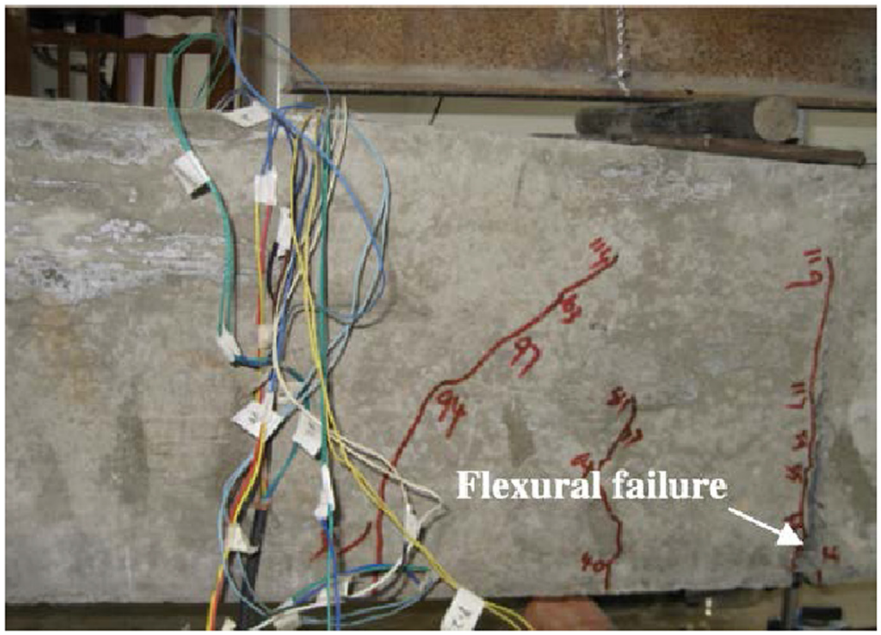

(b)

Fig. 12. Crack patterns of beam SR6 obtained by the (a) numerical analysis and (b) experiment [45].

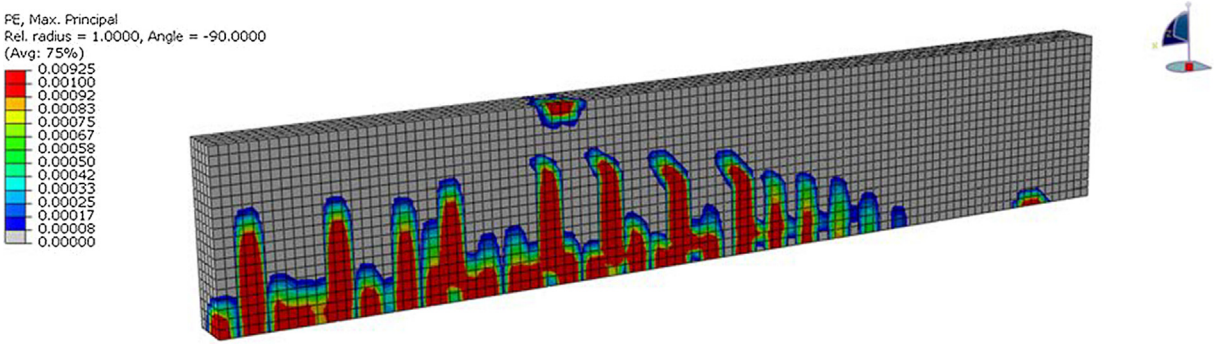

Fig. 13. Crack patterns of beam SS obtained numerically.

middle of the beam and the application of the point load), comprising a large crack near the middle of the beam and another under the applied load. In addition, a number of cracks merge into one large diagonal crack in the high shear region (i.e. the area between the support and the application of the point load). Similarly, in the experimental image, one vertical crack formed in the constant-moment region, another short crack occurred below the applied load and a diagonal crack developed in the high shear region.

Figs. 13 and 14 present the crack patterns obtained numerically for the beams SS and B3, respectively, which are the beams reinforced with stainless steel; the experimental patterns are not included in the literature for these beams. With reference to beam SS, it is observed that a

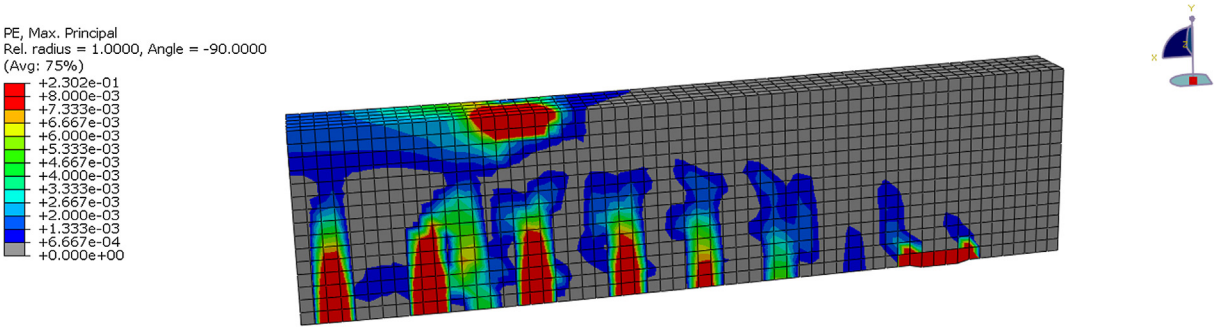

Fig. 14. Crack patterns of beam B3 obtained numerically.

Table 2
Material properties of stainless steel reinforcement included in the study [48].

Stainless steel type	Grade	Bar diameter (mm)	$\sigma_{0.2}$ (N/mm^2)	σ_u (N/mm^2)	E (kN/mm^2)	ε_u (%)	n	m
Austenitic	1.4311 (304LN)	12	480	764	203	38.6	4.7	4.8
Lean duplex	1. 4162 (LDX2101)	12	682	874	199	20.4	5.3	5.0
Austenitic	1.4307 (304L)	12	562	796	210	30.7	4.7	4.8

Table 3
Range of geometrical parameters included in the study.

b (mm)	d (mm)	Bar diameter (mm)
100–150	125–255	8–12

large number of cracks developed, which are well distributed along the length of the beam. On the other hand, in Fig. 14 for beam B3, it is shown that two cracks developed in the constant moment region, one crack beneath the load point and four cracks in the shear region. The fewer number of cracks in this case, compared with SS, are mainly due to the shorter member length.

On the basis of data presented in this and previous sections, it is concluded that the FE model developed in this study is capable of providing a good prediction of the behaviour of stainless steel and carbon steel RC beams in terms of the ultimate load, load-displacement response and crack propagation. There are some very small differences in terms of initial bending stiffness, but this is most likely due to localised cracking in the test which cannot be accurately assessed in the numerical model.

6. Validation of the proposed analytical models

Both the full and simplified analytical models described previously are validated herein using the FE model, by comparing the predicted bending capacities. In order to obtain a robust validation, both of the reinforced concrete beams which included stainless steel rebar, i.e. SS and B3, are studied. A number of different concrete strengths are used in the analysis (i.e. C26, C30, C40, C50). Additionally, three different grades of stainless steel are investigated using the data presented by Gardner et al. [48], which is presented in Table 2. It is noteworthy that the steels are listed giving their European designation (i.e. 1.4XXX) as well as the commonly used AISI names, in brackets. Additionally, both beams B3 and SS are selected for further analysis in which a number of different geometric properties are varied, in order to assess their influence on the response. These parameters are detailed in Table 3.

Tables 4 and 5 present the bending moment capacity obtained from the proposed full analytical method (M_{AM}), the simplified analytical method (M_{SM}) and the numerical analysis (M_{FE}) as well as the values determined using the design method provided in Eurocode 2 (M_{EC2}), for beam SS and B3, respectively. In the Eurocode calculation, it is assumed that the stainless steel material model is elastic-perfectly plastic. In addition, the bending moment capacity predicted using both the full and the simplified analytical solutions are presented together in Fig. 15. This figure also includes the equation for the tendency of the data, as well as the R^2 (coefficient of determination). Based on the data in these tables and Fig. 15, the following general observations are made:

- An excellent agreement is obtained between the numerical analysis and the proposed full analytical method in almost all cases, with the maximum and average M_{AM}/M_{FE} values being −19% and −15.6%, respectively, for beam SS and −13% and −4.3%, respectively, for beam B3. These same values using the Eurocode 2 design rules

Table 4
Comparison between the ultimate bending moment capacity of the numerical and that of the analytical analysis for beam SS.

Stainless steel grade	Bar diameter (mm)	Concrete grade	M_{EC2} (kNm)	M_{AM} (kNm)	M_{FE} (kNm)	M_{SM} (kNm)	M_{EC2}/M_{FE} (%)	M_{AM}/M_{FE} (%)
1.4311 (304LN)	12	30	26.15	31.95	39.56	30.20	−33.89	−19.23
		40	26.53	33.44	41.11	32.25	−35.47	−18.67
		50	26.76	34.49	42.20	34.04	−36.59	−18.27
1. 4162 (LDX2101)	12	30	36.23	40.01	45.79	39.35	−20.88	−12.62
		40	37.00	41.78	47.21	41.88	−21.63	−11.51
		50	37.47	42.92	48.37	44.01	–22.54	−11.27
1.4307 (304L)	12	30	30.30	35.13	42.36	33.76	−28.48	−17.07
		40	30.83	36.66	43.71	35.88	−29.47	−16.13
		50	31.15	37.69	44.87	37.70	−30.58	−16.01
Average value							−28.8	−15.6
Correlation coefficient							0.952	0.995

Table 5
Comparison between the ultimate bending moment capacity of the numerical and that of the analytical analysis for beam B3.

Stainless steel grade	Diameter (mm)	Concrete grade	M_{EC2} (kNm)	M_{AM} (kNm)	M_{FE} (kNm)	M_{SM} (kNm)	M_{EC2}/M_{FE} (%)	M_{AM}/M_{FE} (%)
1.4362 (AIS 2304)	8	26.6	10.45	9.79	11.12	10.45	−6.03	−11.92
		40	11.61	11.84	12.32	11.68	−5.76	−3.90
1.4311 (304LN)	12	26.6	11.51	11.37	11.54	11.65	−0.26	−1.49
		40	12.38	13.50	15.11	12.94	−18.06	−10.64
1. 4162 (LDX2101)	12	26.6	13.11	12.33	11.43	13.11	14.70	7.88
		40	16.55	15.98	17.32	16.69	−4.43	−7.73
1.4307 (304L)	12	26.6	12.95	11.98	11.22	12.98	15.42	6.81
		40	14.15	14.78	17.02	14.52	−16.86	−13.16
Average value							−2.7	−4.3
Correlation coefficient							0.768	0.923

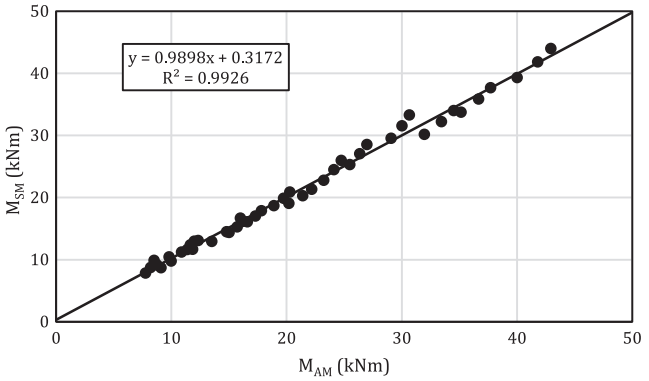

Fig. 15. Comparison between the results obtained using the full and simplified analytical solution.

Table 6
Rebar stresses compared to their proof stresses for beam B3.

Grade of stainless steel	Reinforcement diameter (mm)	Concrete grade	Stress in the reinforcement (N/mm^2)	Reinforcement proof strength (N/mm^2)
1.4362 (AIS 2304)	8	26.6	879.88	1003
		40	1023.88	1003
1.4311 (304LN)	12	26.6	472.79	480
		40	529	480
1. 4162 (LDX2101)	12	26.6	525.63	682
		40	652.72	682
1.4307 (304L)	12	26.6	505.74	562
		40	590.24	562

(M_{EC2}/M_{FE}) are −37% and −28.8% for SS and −18% and −2.7% for B3. Clearly, the full analytical design method, based on determination of limiting deformations, provides more accurate and realistic moment capacities.

- For beam SS (Table 4) the full analytical method underestimates the bending moment capacity in all cases, similarly for beam B3 (Table 5), the predicted analytical results are below the numerical results in all cases, except two values.
- For beam SS, it can be seen that the proposed full analytical method improves the bending capacity of the section in average by around 19.0% compared to the current design approach in EC2 whilst no improvement is found for beam B3. In the latter case, the relatively lower prediction using the analytical model rather than existing design rules in some cases is due to the fact that the stresses in the rebar are lower than their proof stress, as shown by the values presented in Table 6, when the beam reaches to the maximum loading capacity. Therefore, these beams were not designed to exploit the strain hardening qualities of the stainless steel as concrete failure dominates. With reference to Fig. 15, it is observed that the predictions of the bending moment capacity obtained using the simplified analytical solution are in very good agreement with those obtained using full analytical solution. In all cases, the simplified predictions fluctuate above and below the prediction of the full analytical model. Therefore, it is concluded that the simplified solution is adequate for predicting the bending moment capacity for stainless steel RC beams.

By implementing these proposed analytical solutions for the design of concrete beams reinforced with stainless steel, the distinctive strain hardening properties of stainless steel are exploited, thus improving the capacity and ductility of the beams in design. It is unlikely that the full strain hardening capacity of stainless steel would be utilised in real structures as failure by concrete crushing is likely to develop first. Nevertheless, the results presented in Tables 4 and 5 illustrate the capability of the proposed methods for providing a more accurate and efficient bending moment capacity over a wide range of concrete strengths and stainless steel grades, compared to the traditional design method.

7. Conclusions

This paper has presented a detailed study into the behaviour of stainless steel reinforcement in concrete structures. A strong case was presented for why stainless steel can provide a legitimate solution for some of the most common and expensive challenges associated with concrete infrastructure, i.e. degradation of the steel reinforcement. Stainless steel is a very ductile material that has distinctive characteristics such as corrosion and fire resistance, durability and sustainability. There are two main barriers to more widespread use of stainless steel rebar in construction. Firstly, there is a perception amongst engineers that it is prohibitively expensive. Although stainless steel is undoubtedly more expensive than carbon steel in terms of initial costs, over the life time of a structure if maintenance and rehabilitation works can be avoided through the use of more durable materials, then stainless steel provides a very competitive and efficient design option. This is certainly an area that warrants a more detailed analysis, once efficient design rules have been established. Secondly, there is a huge dearth of useful design data and guidance to assist engineers in the specification of stainless steel reinforced concrete. Current design codes such as Eurocode 2 do not include specific guidance for stainless steel and therefore ignore the significant strain hardening characteristics and high levels of ductility that it offers. This design approach provides inaccurate strength capacity predictions. Therefore, the current study implements the Continuous Strength Method into the design of RC beams including full and simplified approach which incorporates the distinctive characteristic of stainless steel in design of reinforced concrete beams reinforced stainless steel. The FE model is developed and validated using the available data in the literature. Then, it is used to validate the proposed analytical solution and to generate a parametric

study. The key influential parameters are analysed and it is shown that the full and simplified analytical solutions provide a reliable means for predicting the capacity of beam. These equations can be used by engineers wishing to include stainless steel reinforced concrete in their designs, without the inefficiencies of existing methods.

Appendix A. Supplementary material

Supplementary data to this article can be found online at https://doi.org/10.1016/j.engstruct.2019.109432.

References

[1] Evans K. RB Rebak in Corrosion Science–A Retrospective and Current Status in Honor of Robert P, Frankenthal, PV, 13; 2002. p. 344–54.
[2] Baddoo NR. Stainless steel in construction: a review of research, applications, challenges and opportunities. J Constr Steel Res 2008;64(11):1199–206.
[3] Gardner L. The use of stainless steel in structures. Prog Struct Mat Eng 2005;7(2):45–55.
[4] Yang L, Zhao M, Xu D, Shang F, Yuan H, Wang Y, et al. Flexural buckling behaviour of welded stainless steel box-section columns. Thin-Walled Struct 2016;104. pp. 185–197.00.
[5] Hassanein M, Silvestre N. Flexural behavior of lean duplex stainless steel girders with slender unstiffened webs. J Constr Steel Res 2013;85:12–23.
[6] Wang Y, Yang L, Gao B, Shi Y, Yuan H. Experimental study of lateral-torsional buckling behavior of stainless steel welded I-section beams. Int J Steel Struct 2014;14(2):411–20.
[7] Gardner L, Theofanous M. Discrete and continuous treatment of local buckling in stainless steel elements. J Constr Steel Res 2008;64(11):1207–16.
[8] Huang Y, Young B. Design of cold-formed lean duplex stainless steel members in combined compression and bending. J Struct Eng 2014;141(5):04014138.
[9] Afshan S, Gardner L. The continuous strength method for structural stainless steel design. Thin-Walled Struct 2013;68:42–9.
[10] Ramberg W, Osgood WR. Description of stress-strain curves by three parameters. Issue 902 of National Advisory Committee for Aeronautics Technical Note; 1943.
[11] Rasmussen KJR. Full-range stress–strain curves for stainless steel alloys. J Constr Steel Res 2003;59(1):47–61.
[12] Pérez-Quiroz J, Terán J, Herrera M, Martínez M, Genescá J. Assessment of stainless steel reinforcement for concrete structures rehabilitation. J Constr Steel Res 2008;64(11):1317–24.
[13] British Highways Authority. Advice note: Design manual for roads and bridges BA84/02: The use of stainless steel reinforcement in highway structures; 2003. Available at: < https://www.bssa.org.uk/cms/File/REBar%20report.pdf > [Accessed 5 March 2019].
[14] Cramer S, Covino B, Bullard S, Holcomb G, Russell J, Nelson F, et al. Corrosion prevention and remediation strategies for reinforced concrete coastal bridges. Cem Concr Compos 2002;24(1):101–17.
[15] Briz E, Biezma M, Bastidas D. Stress corrosion cracking of new 2001 lean–duplex stainless steel reinforcements in chloride contained concrete pore solution: an electrochemical study. Constr Build Mater 2018;192:1–8.
[16] Gardner L, Nethercot DA. Structural stainless steel design: a new approach. J Struct Eng 2004;82(21):21–30.
[17] Gardner L, Yun X, Macorini L, Kucukler M. Hot-rolled steel and steel-concrete composite design incorporating strain hardening. Structures 2017;9:21–8.
[18] Shamass R, Cashell KA. Analysis of stainless steel-concrete composite beams. J Constr Steel Res 2018;152:132–42.
[19] British Stainless Steel Association. The use of stainless steel reinforcement on bridges; 2003. Available at: < http://www.bssa.org.uk/cms/File/REBar%20report.pdf > [Accessed 11 April 2017].
[20] McGurn J. Stainless steel reinforcing bars in concrete. In: Proceedings of the International Conference of Corrosion and Rehabilitation of Reinforced Concrete Structures, Orlando, FL, FHWA; 1998.
[21] Nickel Institute. Progreso pier built with nickel-containing stainless steel; 2018. Available at: < https://www.nickelinstitute.org/media/2541/progresopierrepackagefb.pdf > [Accessed 11/04 2019].
[22] Thousandswonder. Stonecutters Bridge; 2015. Available at: http://www.thousandwonders.net/Stonecutters+Bridge [Accessed 10 April 2017].
[23] Edvardsen C. Tailor-made concrete structures – case studies from projects worldwide; 2008. Available at: < http://www.abece.com.br/web/restrito/restrito/pdf/ch011.pdf > [Accessed 5 March 2017].
[24] Ashraf M, Gardner L, Nethercot DA. Structural stainless steel design: resistance based on deformation capacity. J Struct Eng 2008;134(3):402–11.
[25] Gardner L. The continuous strength method. In: Proceedings of the institution of civil engineers – structures and buildings, 2008, vol. 161(3). p. 127–33.
[26] Gardner L, Wang F, Liew A. Influence of strain hardening on the behavior and design of steel structures. Int J Struct Stab Dyn 2011;11(05):855–75.
[27] Liew A, Gardner L. Ultimate capacity of structural steel cross-sections under compression, bending and combined loading. Structures 2015;1:2–11.
[28] Su M, Young B, Gardner L. The continuous strength method for the design of aluminium alloy structural elements. Eng Struct 2016;122:338–48.
[29] Lan X, Chen J, Chan T, Young B. The continuous strength method for the design of high strength steel tubular sections in compression. Eng Struct 2018;162:177–87.
[30] Theofanous M, Propsert T, Knobloch M, Gardner L. The continuous strength method for steel cross-section design at elevated temperatures. Thin-Walled Struct 2016;98:94–102.
[31] Mirambell E, Real E. On the calculation of deflections in structural stainless steel beams: an experimental and numerical investigation. J Constr Steel Res 2000;54(1):109–33.
[32] Abdella K. Inversion of a full-range stress–strain relation for stainless steel alloys. Int J Non Linear Mech 2006;41(3):456–63.
[33] Dassault Systèmes. Abaqus user's Guide Manual [Computer program]; 2016. < http://dixon:2080/texis/search/?query=concrete+material&group=bk&CDB=v2016&submit.x=0&submit.y=0 > .
[34] Shamass R, Cashell K. Behaviour of composite beams made using high strength steel. Structures 2017;12:88–101.
[35] Earij A, Alfano G, Cashell K, Zhou X. Nonlinear three–dimensional finite–element modelling of reinforced–concrete beams: computational challenges and experimental validation. Eng Fail Anal 2017;82:92–115.
[36] George J, Rama JK, Kumar MS, Vasan A. Behavior of plain concrete beam subjected to three point bending using concrete damaged plasticity (CDP) model. Mater Today: Proc 2017;4(9):9742–6.
[37] Fan S, Tan KH, Nguyen MP. Numerical model to determine shear capacity of reinforced concrete deep beams exposed to fire. In: High tech concrete: where technology and engineering meet. Springer; 2018. p. 1410–9.
[38] Solhmirzaei R, Kodur V. Modeling the response of ultra high performance fiber reinforced concrete beams. Procedia Eng 2017;210:211–9.
[39] EN 1992-1-1. 'Eurocode 2: Design of concrete structures part 1-1: General rules and rules for buildings. European Committee for Standardization (CEN); 2004.
[40] Wang T, Hsu TT. Nonlinear finite element analysis of concrete structures using new constitutive models. Comput Struct 2001;79(32):2781–91.
[41] Kmiecik P, Kamiński M. Modelling of reinforced concrete structures and composite structures with concrete strength degradation taken into consideration. Arch Civil Mech Eng 2011;11(3):623–36.
[42] Dede T, Ayvaz Y. Nonlinear analysis of reinforced concrete beam with/without tension stiffening effect. Mater Des 2009;30(9):3846–51.
[43] Medina E, Medina JM, Cobo A, Bastidas DM. Evaluation of mechanical and structural behavior of austenitic and duplex stainless steel reinforcements. Constr Build Mater 2015;78:1–7.
[44] Alih S, Khelil A. Behavior of inoxydable steel and their performance as reinforcement bars in concrete beam: experimental and nonlinear finite element analysis. Constr Build Mater 2012;37:481–92.
[45] Dong J, Wang Q, Guan Z. Structural behaviour of RC beams with external flexural and flexural–shear strengthening by FRP sheets. Compos B Eng 2013;44(1):604–12.
[46] Alfano G, De Cicco, Ph. Fiorenzo D, Prota A. Intermediate debonding failure of RC beams retrofitted in flexure with FRP: experimental results versus prediction of codes of practice. J Compos Constr 16(2); 2011:185–95.
[47] Obaidat YT, Heyden S, Dahlblom O, Abu-Farsakh G, Abdel-Jawad Y. Retrofitting of reinforced concrete beams using composite laminates. Constr Build Mater 2011;25(2):591–7.
[48] Gardner L, Bu Y, Francis P, Baddoo NR, Cashell KA, McCann F. Elevated temperature material properties of stainless steel reinforcing bar. Constr Build Mater 2016;114:977–97.